SAND2022-2303C

WEIMOS: Shear Behaviors of Bedded Salt Clay Seams and Their Impact on Disposal Room Porosity

Steven R. Sobolik[1], Chet Vignes[1*], Stuart Buchholz[2], Evan Keffeler[2], Benjamin Reedlunn[1*]*

[1]Sandia National Laboratories, Albuquerque, NM, USA; [2]RESPEC, Rapid City, SD, USA;

** srsobol@sandia.gov*

ABSTRACT: This paper presents laboratory experiments on clay seams in-between layers of salt, and simulations of WIPP disposal rooms that include clay seams. The experiments involved two series of direct shear tests. The first test series was performed on representative core samples from a potash mine near the WIPP. These natural geologic contacts had intergrown halite crystals, and their residual shear strengths were like that of intact salt. The second test series involved artificial clay seams prepared by mixing brine with bentonite, placing the clay between two cylindrical salt specimens with grooved contact surfaces, and hydrostatically consolidating the assembled specimen. The artificial clay seam residual shear behavior was similar to that of a saturated, highly consolidated, clay. Thus, these weak and strong residual strengths likely bound the actual shear behavior of clays seams in bedded salt. The bounds were then used in simulations that probe the sensitivity of WIPP disposal room porosity to clay seam shear behavior. Weaker clay seams accelerated the decrease of room porosity within the first 300 years but had minimal impact on final room porosity.

1 Introduction

Sandia National Laboratories (SNL) is responsible for modeling the long-term behavior of the Waste Isolation Pilot Plant (WIPP), a permanent disposal site in bedded salt for defense-generated transuranic waste. In addition, SNL participates in extensive international collaborations to better understand the behavior of salt for potential spent nuclear fuel repositories. One key subject area for the modeling of the mechanical behavior of emplacement drifts is the influence of inhomogeneities, specifically interfaces between the host salt and other in situ materials such as clay seams within bedded salt. The potential increases in closure rate, roof collapse, and permeability near and along these inhomogeneities are thought to be first-order effects. Despite their importance, characterizations of the peak and residual shear strengths, and permeability of interfaces in salt are extremely rare in the published literature. Minkley and Mühlbauer (2007) documented direct shear laboratory tests on carnallite and salt blocks under varying normal and shear loads and shear velocities, but they did not perform experiments on clay seams.

This paper presents results from laboratory experiments and numerical simulations involving clay seams. The experiments measured the mechanical behavior of a clay seam as it was sheared. Two series of laboratory direct shear tests were performed (Sobolik et al., 2019 & 2020; Keffeler et al., 2021): one involved clay seams from a potash mine near the WIPP, the other involved artificial clay seams. These tests were performed as part of the US-German collaborative Joint Project WEIMOS (2016 – 2019; “Further Development and Qualification of the Rock Mechanical Modeling for the Final HAW Disposal in Rock Salt”) (Lüdeling et al.,

2018). The numerical simulations used the test results to investigate the impact of clay seam shear behavior on the short-term and long-term porosity of disposal rooms at the WIPP.

2 First series of shear tests on interfaces

An initial series of laboratory direct shear tests was performed on several samples of materials assumed to be typical of WIPP emplacement rooms (Buchholz, 2019; Sobolik et al., 2019). Samples with halite-anhydrite and halite-polyhalite interfaces were included in this test series, but this paper will focus on the samples with halite-clay interfaces and pure salt samples. The direct shear test method was designed to measure the complete shear stress-strain curve and characterize the following mechanical properties:

- Intact normal and shear stiffness
- Dependence of shear yield, ultimate, and residual strength on normal stress
- Residual normal and shear stiffness

Sample collection was conducted in a salt-potash mine in the Permian Basin in New Mexico. These samples were to be drilled from the floor of an inclined drift at the mine. Cores were drilled using a concrete coring rig with a diamond bit core barrel having dimensions of 300 mm in diameter and 560 mm long. Several cores were drilled from the floor as planned, but nearly all exhibited damaged seams or interfaces, making them unsuitable for testing. As a result, a determination was made to extract cores horizontally from the rib. This procedure was much more successful; several intact cores were extracted for all the desired interface types.

Four-inch (100-mm) diameter cylindrical specimens were subcored from the field core using a vertical mill. Bright-Cut NHG metal working fluid was used as a lubricant during subcoring to prevent washing of the evaporite materials. The long axes of the subcores were oriented perpendicular to the geologic interface to the extent possible. The subcores were trimmed so that the specimen length on either side of the interface was between 50 and 76 mm. Total specimen length did not exceed 152 mm. The specimens were then cleaned using an alcohol-based degreaser. The interface between the halite layer and the clay section was somewhat well-defined visually when looking at the exterior surface of the sample. In addition to the cores obtained from the Permean Basin mine, RESPEC obtained sections of nominally 4-inch (102-mm) diameter core from a Prairie Evaporite storage well in Alberta, Canada. These samples were used for the initial tests to qualify the test conditions and procedures.

The shear tests were performed using a rock direct shear testing machine designed and fabricated by RESPEC (see Figure 1 for a schematic). It has an axial and shear load capacity of 30,000 pounds (130 kN) each. The machine consists of shear boxes (that hold the test specimen), a normal load ram, a shear load ram, and hydraulic controls. The shear displacement δ is measured by using a linear variable displacement transformer (LVDT). The shear load S is controlled by a mechanical-over-hydraulic intensifier that advances the shear load ram at a set displacement rate. The normal load N is controlled by a pressure regulator that maintains N within 1 percent of the set point. Both maximum shear strength and residual shear strength were determined for each rock type. The tests were conducted at several normal and shear loads up to expected in situ pre-mining stress conditions, and at a single shear velocity of $\dot{\delta} =$ 0.01 in/min (0.0042 mm/sec). This shear velocity is currently the slowest capable on this direct shear machine (and much faster than the $\dot{\delta} =$ 0.00005 to 0.002 mm/sec used by Minkley and Mühlbauer), so these tests were unable to evaluate potential velocity-

dependent shear stress evolution. The tests were performed while holding the load normal to the interface constant. Each test used one of four different normal loads, which corresponded to nominal normal stresses of $\Sigma =$ 3.4, 6.8, 10.3, 16.6 MPa.

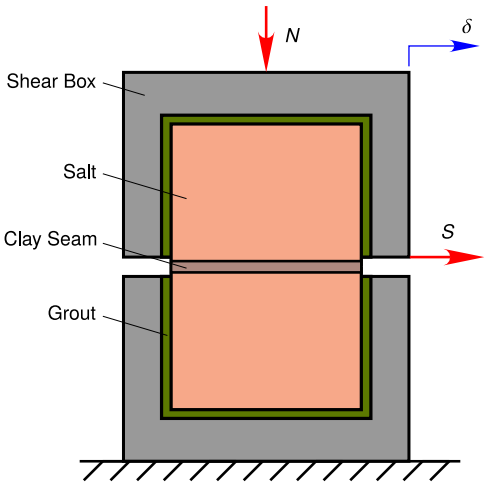

Figure 1. Schematic of direct shear test setup.

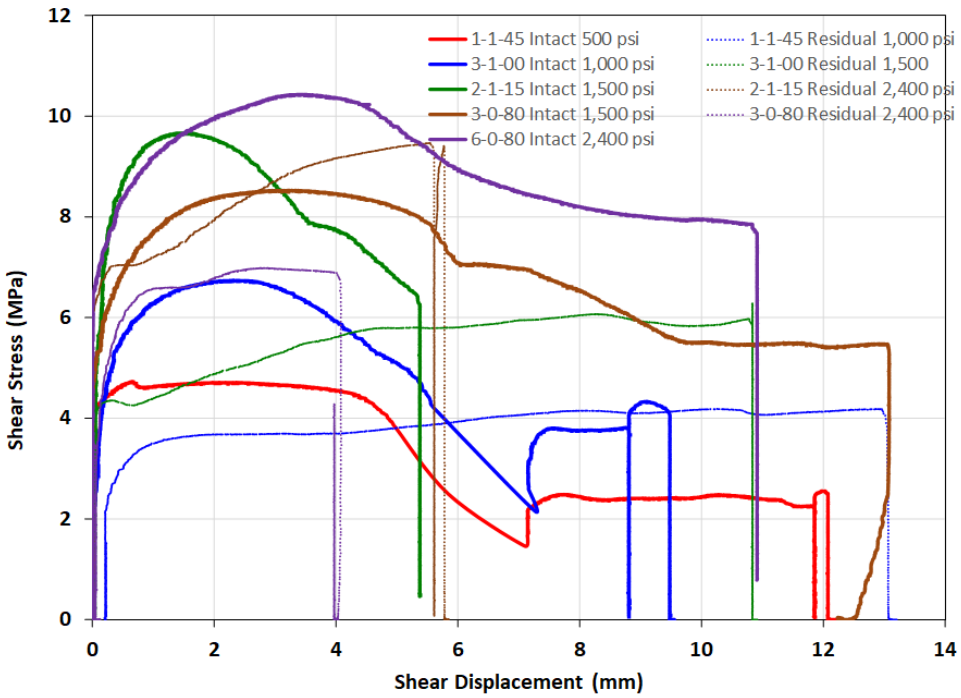

Figure 2. Shear stress vs. displacement for Halite-Clay shear tests.

Regardless of the rock type (i.e., with or without contacts), the specimens behaved and broke like solid salt rock. The tests tended to follow a similar pattern – an increase of shear stress until a break occurred, followed by a sudden drop in stress to an eventual residual value. Figure 2 plots shear stress vs. shear displacement for the tests performed on halite-clay contact samples. The stresses were calculated using the original cross-sectional area of the

interface. See Table 2 in Sobolik et al., (2019) for the peak nominal shear stress and residual nominal shear stress from each experiment.

3 Second series of shear tests on artificial clay seams

A series of laboratory experiments was performed that consisted of fabricating consolidated clay seams within salt (predominately halite) and performing direct shear tests on those clay seams. These tests were conducted at several normal and shear loads up to the expected in situ pre-mining stress conditions, and at the same single shear ram advancement velocity of 0.01 in/min (0.004 mm/sec).

A total of eight artificial clay seam specimens were created. The salt on either side of the clay seam was from the same set of cores extracted for the earlier interface shear tests. A full description of the test procedure is included in Sobolik et al. (2020) and Keffler et al. (2021). The specimen preparation method is summarized as:

1. 4-inch (108 mm)-diameter by approximately 3-inch (76 mm)-long salt cylinders were subcored from the 12-inch-diameter core obtained from the potash mine near WIPP.
2. A series of 1.3-mm-deep circular grooves were machined, radially spaced ~6 mm apart, into one face of each subcore, as shown in Figure 3.
3. Bentonite powder was mixed with saturated salt (halite) brine to a fresh-water moisture content (by weight) of approximately 60 percent.
4. A 6-mm or 12-mm-thick layer of the bentonite-brine mix was applied to the grooved surface of a subcore. A second subcore was placed onto the bentonite-brine mix with the grooved surface facing the bentonite-brine mix. This assembly constituted an unconsolidated test specimen.
5. The unconsolidated test specimen was wrapped in filter fabric and placed into a consolidation vessel. The specimen was protected from the confining oil using neoprene jackets, and the platens were vented to the atmosphere.
6. The test specimen was consolidated under an isostatic stress of 20 MPa (nominal) at 21 degrees Celsius (°C) for 14 days. (For comparison, the lithostatic pressure at the WIPP horizon is approximately 14.8 MPa.) Excess pore fluid from the bentonite mixture was expelled through the vents.
7. The consolidated test specimen was removed from the consolidation vessel, and the diameter of the clay seam was measured. The consolidated test specimens were coated in clear acrylic to protect them from the encapsulation grout used in the shear boxes. An example photograph of a consolidated specimen is provided in Figure 3.

Four of the specimens had pre-consolidation seam thicknesses of 6 mm, and the remaining four had pre-consolidation seam thicknesses of 12 mm. The post-consolidation seam thicknesses were approximately 1.6 mm and 4.8 mm for the 6- and 12-mm pre-consolidation seam thicknesses, respectively. After the shear tests, clay chips from the specimens were tested for moisture content; this ranged from 13 to 17%. Post-test examination also revealed that there was no asperity-to-asperity contact between the two machined ends of the salt at the seam.

Shear tests were performed at three normal loads that corresponded to nominal normal stresses of 3.4, 6.8 and 10.3 MPa (500, 1000, 1500 psi). The data from each test were analyzed to determine the following:

- Pretest normal stiffness
- Pretest shear stiffness
- Peak shear strength

- Shear strength at 0.75 inch (19 mm) of shear displacement (a proxy for residual strength)
- Posttest shear stiffness
- Posttest normal stiffness.

For the study of seam shear behavior, the peak and residual shear strength are of highest importance. Nominal stresses were calculated using the original shear area of the specimens.

Figure 3. Photographs of grooves machines into salt sample, and consolidated test specimen.

One source of error was the shear displacement δ, causing the top half of the specimen to protrude over the bottom half. The maximum shear displacement reached as high as 20 mm (0.80 inch). This overhang led to a decrease in modified cross-sectional area A_δ available to resist the normal and shear loads. This modified cross-sectional area can be calculated as the overlap between two offset circles as

$$A_\delta = (\theta - \sin\theta)\left(\frac{d_0}{2}\right)^2,\ \theta = 2\cos^{-1}\frac{\delta}{d_0}, \quad (2)$$

where d_0 is the initial specimen diameter. Nevertheless, the nominal normal and shear stresses were calculated assuming the initial area of the specimens $A_0 = \pi\ d_0^2 / 4$. The error that results from assuming constant area is negligible for the intact portion of the tests as shear displacement is small prior to exceeding the ultimate shear strength of the specimens. For the portions of the intact tests after seam fracture (ultimate shear strength), the shear displacement and area loss are larger; neglecting the changing area resulted in roughly 15-25% errors in calculated stresses at the end of the test. In the Mohr-Coulomb strength criterion fits discussed below, calculations of shear stress calculated with original and modified contact area are compared.

Figure 4 plots the shear stress versus shear displacement curves for the intact sample tests 6A/6B and 7A/7B, which were performed at a nominal normal stress of 6.83 MPa for the 6-mm and 12-mm pre-consolidated seams, respectively. For the plots in Figure 4, two values are plotted for shear stress: the blue curves represent shear stress calculated with the original seam contact area, A_0 , calculated with the average original seam diameter d_0; and the orange curves represent the shear stress calculated using the modified contact area reduced by the shear displacement, A_δ.

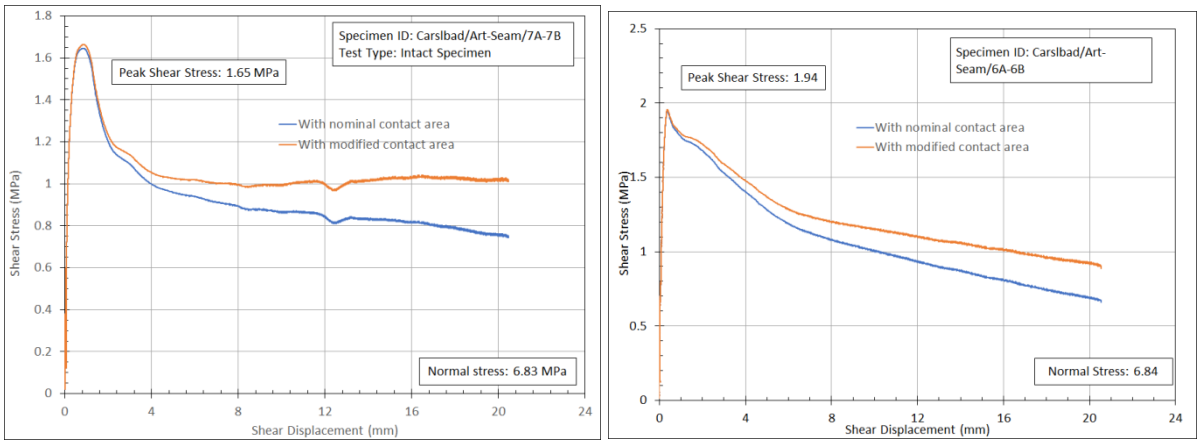

Figure 4. Shear Stress vs. Shear Displacement for Nominal Normal Stress of 6.89 MPa, pre-consolidation seam thicknesses of 6 mm (left), 12-mm (right)

In the initial analysis of all eight tests using the original seam contact area, two tests at most appeared to have achieved a residual shear stress through 19 mm shear displacement. After recalculating the shear stress based on the displacement-reduced contact area, four tests appear to have achieved a residual stress: Tests #8, #2, #4, and #7. It is unclear why the other tests failed to reach a residual stress condition.

While calculating the shear stress using the displacement-reduced contact area indicated that four of the shear tests reached a residual shear stress, that same method changes the calculation of the normal stress during the test. As the normal force remains essentially constant, the reduction in area causes an increase in normal stress on the contact area by about 33%. This is a curious result, because there is no corresponding increase in the shear stress with increasing Cauchy normal stress. This result complicates the notion that the shear tests actually reached a residual shear stress and somewhat skews any analysis of the shear behavior. For now, the post-test analysis simply utilizes the final shear strength measured at 19 mm of shear displacement.

A summary of the measured peak and residual shear stresses for all the tests is listed in Table 1, with shear stress values at δ=19 mm based on the modified contact area A_δ.

Table 1. Direct shear testing strength results for artificial seam samples.

Specimen/ Test ID	Pre-Consolidation Seam Thickness (mm)	Nominal Normal Stress, psi (MPa)	Peak Nominal Shear Stress, psi (MPa)	Shear Stress, psi (MPa), at 0.75” (19 mm) Displ.
1A-1B	6	504 (3.47)	140 (0.97)	96 (0.66)
2A-2B	6	1494 (10.3)	325 (2.24)	161 (1.11)
3A-3B	12	1000 (6.89)	215 (1.48)	76 (0.52)
4A-4B	12	507 (3.50)	277 (1.91)	104 (0.72)
5A-5B	12	1487 (10.3)	427 (2.94)	155 (1.07)
6A-6B	6	992 (6.84)	282 (1.94)	136 (0.94)
7A-7B	12	990 (6.83)	239 (1.65)	149 (1.03)
8A-8B	6	496 (3.42)	234 (1.61)	144 (0.99)

4 Interpretation of test data

The experimental data was analyzed using the Mohr-Coulomb shear strength criterion. This criterion is defined as

$$T = \Sigma \tan \Theta + S_0 \quad (1)$$

where T is either the peak shear stress at failure or the residual shear stress, Σ is the normal stress on the shear surface, Θ is the friction angle, and S_0 is the cohesion strength. All stresses in (1) are taken as nominal stresses (force divided by original cross-sectional area) for simplicity. The friction angle and cohesion strength were fit, in a least squares sense, against the set of tests on each specimen type.

The peak and residual nominal shear stress measurements versus the nominal normal stress, the Mohr-Coulomb fits, and the associated Mohr-Coulomb parameters are shown in Figure 5 and 6. The simple fits reasonably capture each interface type. Notably, the cohesion strength is non-zero in all cases, suggesting the interfaces have a non-zero shear strength at zero normal stress.

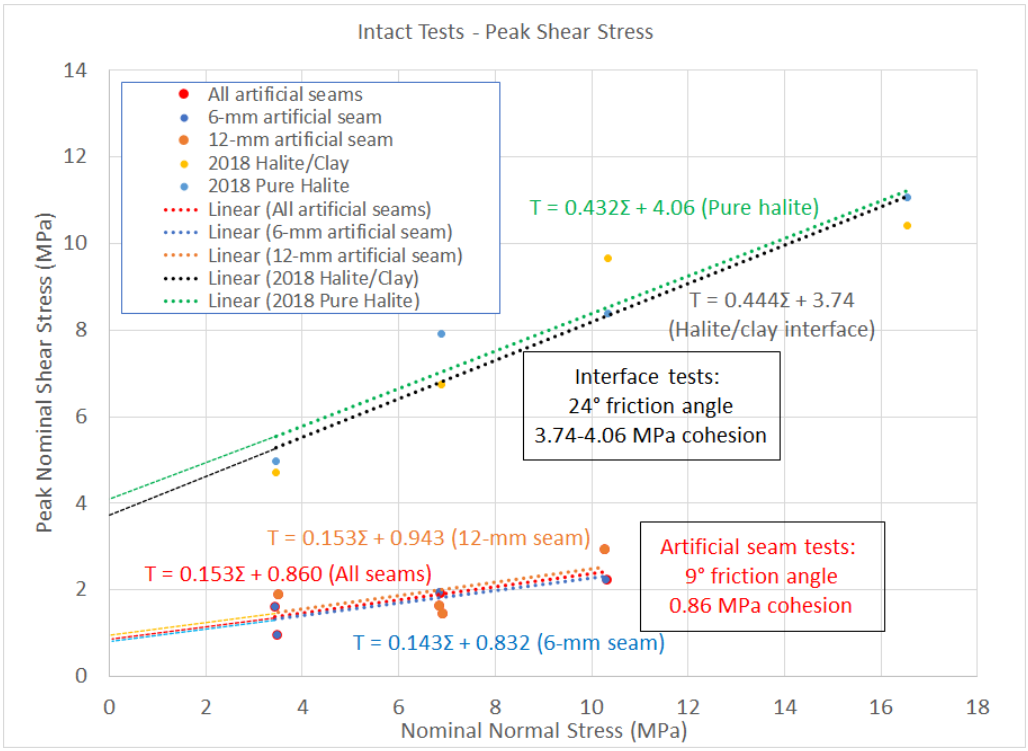

Figure 5. Peak shear stress as function of normal stress, halite interface tests and artificial seam tests.

Figures 5 and 6 show the natural clay seams had shear strengths like that of pure salt, meaning the clay interspersed in the natural clay seams did not weaken the salt. Presumably, a more distinct natural clay seam without intergrown halite crystals would exhibit substantially lower shear strengths. Efforts to extract such seams are ongoing.

Figure 5 and 6 also show the artificial clay seam shear strengths were much lower than those from the previous salt interface tests. The residual strength friction angle is 22.7 / 1.6 = 14 times smaller in the artificial clay seams than the diffuse natural clay seams. For an additional

reference point, a friction coefficient of 0.2, which is equivalent to Φ = 11.3° and S_0=0, has historically been assumed in WIPP geomechanical analyses.

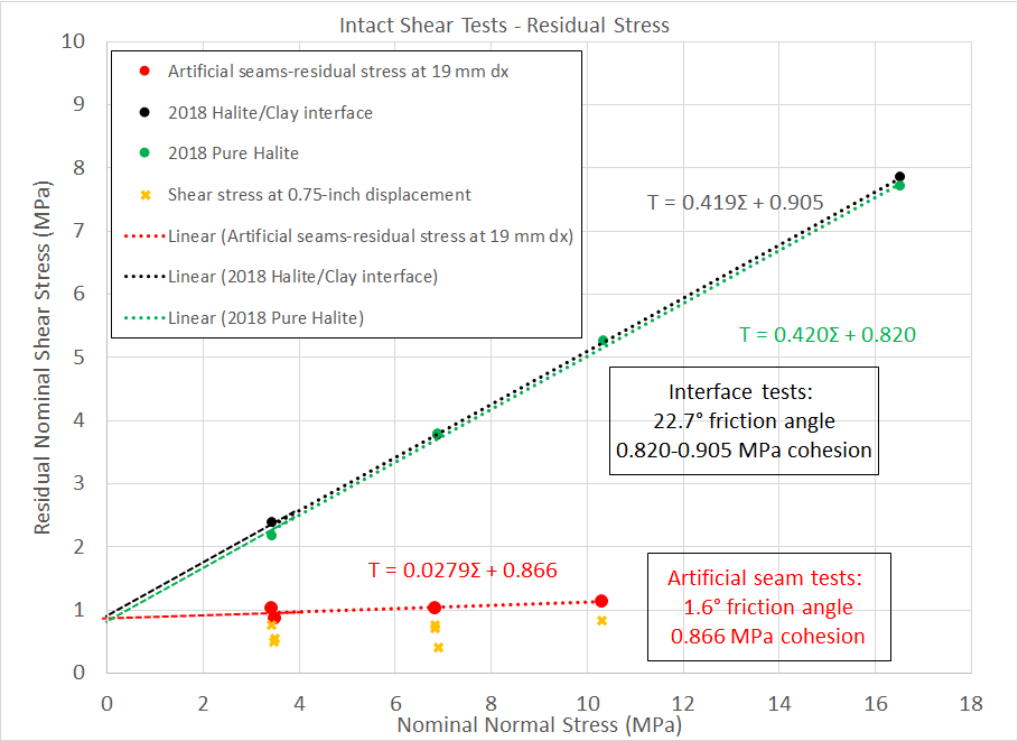

Figure 6. Residual shear stress as function of nominal normal stress, natural halite interface tests and artificial seam tests.

The softness of clay and small asperity size in the artificial clay seams may explain the low Mohr-Coulomb parameter measurements, particularly the friction angles. When examining the collection of artificial seam tests, it was surprising that the 6-mm and 12-mm artificial seams underwent approximately the same behavior, with similar Mohr-Coulomb cohesion and friction angle values. This suggests that the tests may be measuring the shear strength of the clay, rather than the shear strength of a rougher clay-salt interface where the salt must deform somewhat to permit sliding. It is assumed that no salt asperity-to-salt asperity contact occurred during shearing and the behavior was likely dominated by the saturated, consolidated, clay properties. This conclusion is supported by the calculated values of the Mohr-Coulomb constants. Clays (especially over-consolidated clays) typically exhibit non-zero cohesion. The values of cohesion in Figure 6 are larger than most references cite for clays (for example, Ladd & Edgers, 1972), but not dramatically higher. Direct shear tests on clay-only samples would help determine if the clay does, in fact, dominate the shear response.

5 Application to geomechanical analyses

Clay seam sliding at the WIPP site has historically been modeled using Coulomb friction, and the same simple approach is continued herein. Coulomb friction is defined as

$$\tau = \sigma \tan\theta, \tag{2}$$

where τ is the Cauchy shear stress at the interface, σ is the Cauchy normal stress on the interface, and θ is the residual strength friction angle.

This approach ignores the intact peak strength and assumes sliding occurs as soon as the shear stress at the interface reaches the residual shear strength τ. The intact peak strength is assumed to be important only upon room excavation when cracks first form in the clay seams. The remainder of the room closure period will involve crack propagation and sliding along the clay seam. It could be worth trying to incorporate crack propagation, which generally requires less stress than initiation, into a model, but the propagation behavior has not been quantified. Accordingly, it is prudent to assume the propagation strength is equal to the residual strength to begin with.

Expression (2) is similar to (1) except $S_0 = 0$ and the shear and normal stresses are Cauchy stresses. A model with non-zero cohesion strength may be attempted in the future, but if $S_0 = 0$, then the distinction between nominal and Cauchy stresses becomes less relevant because $\theta = \Theta = \tan^{-1}(\tau/\sigma) = \tan^{-1}(T/\Sigma)$.

The Coulomb friction model assumes sliding is a rate independent process, but there may be a shear rate dependence similar to that found by Minkley and Mühlbauer (2007). The experimental shear velocity of 363 mm/day is multiple orders of magnitude above clay seam shear velocities around rooms at the WIPP. WIPP clay seam shear velocities have not been directly measured, but the sliding within one day is not noticeable, so these velocities are probably well beneath 1 mm/day. Future clay seam shear experiments will hopefully include shear velocity sensitivity studies.

Another consideration is whether fluid pressure within an in-situ clay seam would support some of the normal stress, thereby reducing the effective normal stress applied to the clay material. This effect might be significant if the clay provided the majority of the clay seam strength, but, most likely, sliding causes asperities on either side of a clay seam to interlock and supply the bulk of the shear resistance.

The simple clay seam constitutive model in Eqn (2) was utilized in finite element simulations similar to those in Stone (1997), which predicted disposal room porosity over time. Figure 7 shows a schematic of the boundary conditions, stratigraphy, and idealized, homogeneous, block of waste within both upper and lower horizon disposal rooms at the WIPP. This disposal room is long and slender, allowing a plane-strain approximation at room mid-length. Disposal room porosity was computed as

$$\phi = \frac{V_R - V_S}{V_R}, \tag{3}$$

where V_R was the current volume of the room (void space plus solid waste) and V_S was the volume of solid waste within the room. Any gas within the room was allowed to escape, so that the gas pressure remained zero. The most important deviations from Stone (1997), for the purposes of this paper, are these simulations included the 12 clay seams shown in Figure 7 and used an updated waste constitutive model calibration.

The two seams closest to the room are Clay F and G. Clay Seam F is generally several inches wide and resembles the interfaces from the first series of lab tests. Clay Seam G is a thin distinct clay layer that resembles the artificial seams from the second series of lab tests over a few centimeters, yet still exhibits centimeter undulations over spans of several meters. The other clay seams near WIPP are still being studied, but they are expected to be somewhere between Clay F and G. Consequently, Clay F's friction coefficient was set to the upper bound from the shear tests ($\tan\theta = 0.42$), while all other clay seams were varied between the lower

and upper bounds from the shear tests (tan θ = 0.0279 to 0.42) (see Fig. 6). The simulations were run with a coarse mesh to get a preliminary understanding of the clay seam sensitivity.

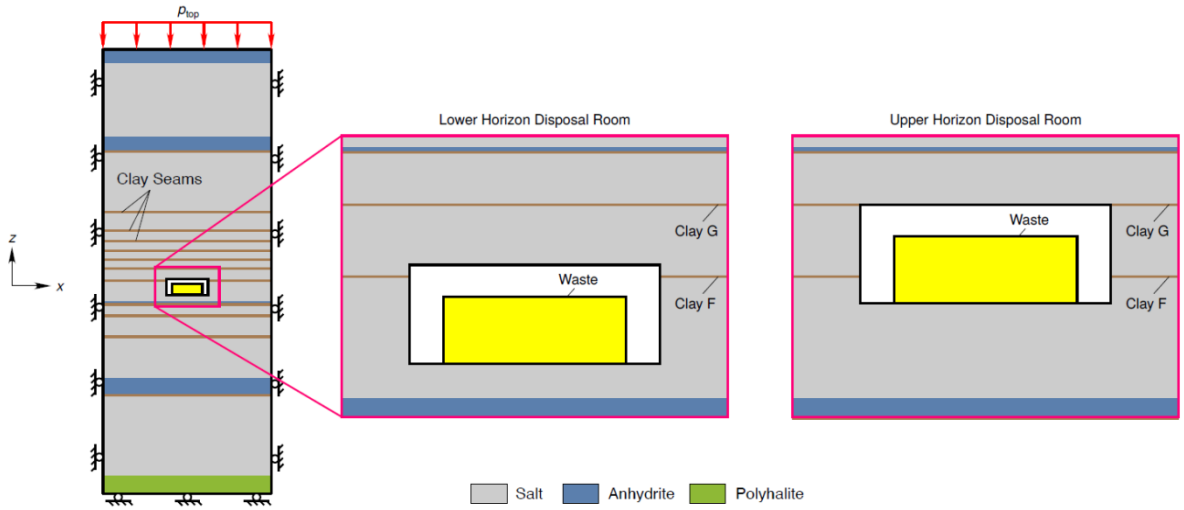

Figure 7. WIPP disposal room simulation boundary conditions and idealized stratigraphy, including seam locations for upper and lower horizon disposal rooms.

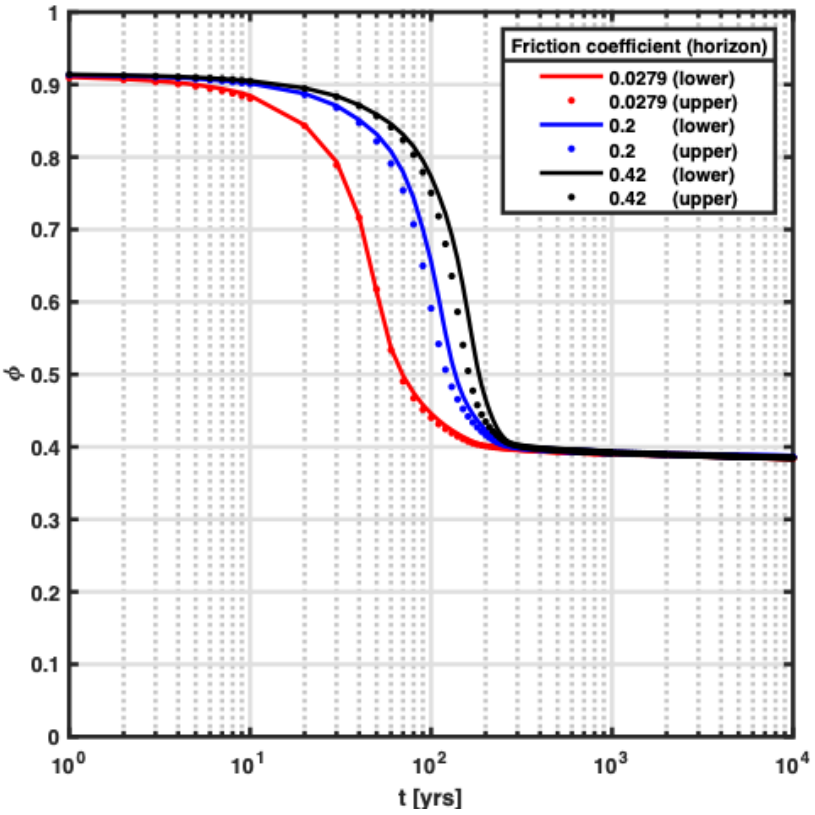

Figure 8. Upper and lower horizon disposal room porosity histories, assuming no gas trapped in the room. The friction coefficient tan θ was varied for all seams except Seam F.

Figure 8 shows the room porosity for upper and lower room configurations for several different friction coefficients for all clay seams, except Clay F. For times less than 300 years, the room porosity is quite sensitive to the clay seam sliding. At 70 years, the porosity varies between

approximately 0.5 and 0.85 when the clay friction coefficient is varied from tan θ = 0.0279 to 0.42. At ~300 years, however, the waste is highly compacted and begins to supply resistance comparable to the far-field lithostatic pressure. As the waste pressure starts to balance with the salt pressure, the clay seam shear stresses asymptote to approximately 0.38 and the room porosity becomes insensitive to the clay seam friction coefficient.

6 Conclusions

Eight samples of salt with artificial clay seams of two different thicknesses were subjected to displacement-controlled direct shear tests at three different normal loads. The tests ran according to procedure, and both maximum shear strength and final shear strength were determined for each test. The test results were similar in that a peak stress was achieved at which the seam broke, and the shear stress lowered through continual shearing. Although none of the tests achieved a true residual stress plateau, the final shear stresses reasonably conformed to Mohr-Coulomb behavior. The Mohr-Coulomb parameters were similar to those of a highly consolidated, saturated, clay, which is to say they were quite low compared to direct salt surface contacts.

These artificial clay seam results and previous direct shear test results on salt with diffuse clay interfaces appear to provide lower and upper bounds for the expected strength of clay seams from the WIPP site. These results will hopefully be precursors to tests on relevant clay seams from the WIPP site (probably Clay Seams F and G). Some potential improvements for future shear tests would be to reduce the shear velocity to something closer to expected in situ rates, use larger diameter samples for more asperity interlocking, and take the evolution of the contact area into account.

The upper and lower bounds from the direct shear tests were used in simulations of waste compaction due to disposal room closure at the WIPP. This preliminary study found disposal room porosity was sensitive to clay seam sliding behavior during the first 300 years, yet became insensitive afterwards.

Acknowledgements

Sandia National Laboratories is a multimission laboratory managed and operated by National Technology and Engineering Solutions of Sandia, LLC., a wholly owned subsidiary of Honeywell International, Inc., for the U.S. Department of Energy's National Nuclear Security Administration under contract DE-NA0003525. This research is funded by WIPP programs administered by the Office of Environmental Management (EM) of the U.S. Department of Energy.

References

BUCHHOLZ, S.A., 2019. Technical Letter Memorandum RSI/TLM-190, Direct Shear Testing of Bedded Interfaces and Clay Seams, RESPEC, Rapid City, SD, January 11, 2019.

HANSEN, F.D., SOBOLIK S.R., & STAUFFER, P., 2016A. Intermediate Scale Testing Recommendation Report, FCRD-UFD-2016- 000030 Rev. 0, SAND2016-9041R, Sandia National Laboratories, Albuquerque, NM.

HANSEN, F.D., STEININGER, W., & BOLLINGERFEHR W., 2016B. Proceedings of the 6th US/German Workshop on Salt Repository Research, Design, and Operation. FCRD-

UFRD-2016-00069. SAND2016-0194R, Dresden, Germany, Sept. 2015. Sandia National Laboratories, Albuquerque, NM.

HANSEN, F.D., STEININGER, W., & BOLLINGERFEHR, W., 2017. Proceedings of the 7th US/German Workshop on Salt Repository Research, Design, and Operation, SFWD-SFWST-2017-000008. SAND2017-1057R, Arlington, VA, Sept. 2016, Sandia National Laboratories, Albuquerque, NM.

KEFFELER, E.R, BUCHHOLZ, S.A., & SOBOLIK, S.R., 2021. Direct Shear Testing of Consolidated Artificial Clay Seams in Salt. ARMA 21-1566. Presented at 55th US Rock Mechanics/Geomechanics Symposium held in Houston, Texas, USA, 20-23 June 2021.

LADD. C.C. AND L. EDGERS, 1972. Consolidated-Undrained Direct-Simple Shear Tests on Saturated Clays. Department of Civil Engineering, Massachusetts Institute of Technology, Cambridge, Res. Rept. R72-82, No. 284, 1972, 354 pp.

LÜDELING, C., SALZER, K., GÜNTHER, R. -M., HAMPEL, A., YILDIRIM, S., STAUDTMEISTER, K., GÄHRKEN, A., STAHLMANN, J., HERCHEN, K., LUX, K.-H., REEDLUNN, B., SOBOLIK, S., HANSEN, F.D. & BUCHHOLZ, S.A. (2018). WEIMOS: Joint Project on further development and qualification of the rock mechanical modeling for the final HLW disposal in rock salt. Overview and first results on tensile stress modeling. Proceedings of the 9th Conference on the Mechanical Behavior of Salt (Saltmech IX), 12-14 Sept. 2018, Hannover, Germany. Eds.: S. Fahland, J. Hammer, F.D. Hansen, S. Heusermann, K.-H. Lux & W. Minkley, published by BGR Hannover, ISBN 978-3-9814108-6-0, pp. 459-477.

MINKLEY, W. & M MÜHLBAUER, J., 2007. Constitutive Models to Describe the Mechanical Behavior of Salt Rocks and the Imbedded Weakened Planes. Wallner, M., K-H Lux, W. Minkley, H.R. Hardy, eds. The Mechanical Behavior of Salt: Understanding of THMC Processes in Salt. Taylor & Francis/Balkema, Leiden, The Netherlands.

SOBOLIK, S.R., KEFFELER, E.R, BUCHHOLZ, S.A., BORGLUM, S. & REEDLUNN, B., 2019. Shear Behavior of Bedded Salt Interfaces and Clay Seams. ARMA 19-040. Presented at 53rd US Rock Mechanics/Geomechanics Symposium held in New York, NY, USA, 23-26 June 2019.

SOBOLIK, S.R., KEFFELER, E.R, & BUCHHOLZ, S.A., 2020. Shear Behavior of Artificial Clay Seams within Bedded Salt Structures. SAND2020-11959, Sandia National Laboratories, Albuquerque, NM, USA.

STONE, C.M., 1997. Final disposal room structural response calculations. SAND97-0795, Sandia National Laboratories, Albuquerque, NM, USA.